Carrier Synchronization of Offset Quadrature Phase-Shift Keying

M. K. Simon[1]

This article contains analyses of the performance of various carrier synchronization loops for offset quadrature phase-shift-keying (OQPSK) modulation, all motivated in one form or another by the maximum a posteriori (MAP) estimation of carrier phase. When they are implemented as either high or low signal-to-noise ratio (SNR) approximations to the generic implementation suggested by the MAP estimation of carrier phase for an OQPSK signal, it is shown that the loops behave more like biphase than quadriphase loops in that they only exhibit a 180-deg phase ambiguity rather than the 90-deg phase ambiguity typical of the latter. This phase ambiguity advantage coupled with the mean-square tracking-error performance advantage that results and its ultimate effect on average error probability performance offer a potentially significant justification for using OQPSK rather than QPSK even on a linear transmission channel, where it often is reasoned (based on the assumption of an ideal environment) that the two modulation schemes perform identically.

I. Introduction

The problem of suppressed-carrier synchronization in digital coherent communication systems has received widespread attention over the years from a theoretical as well as a practical point of view. In reality, these two points of view are not separate from each other in that the carrier synchronization structures that commonly are employed in the design of coherent receivers are those that are motivated by the application of the maximum a posteriori (MAP) estimation theory [1]. A common example of this is the Costas or in-phase–quadrature (I-Q) loop [2,3] for binary phase-shift-keying (BPSK) systems that is derived by suitably using the derivative of the open-loop MAP estimate of carrier phase as the error signal in a closed-loop configuration. Closed loops derived in such a fashion often are referred to as MAP estimation loops [1,4], and this terminology likewise shall be used here in this article. Extension of the above relationship between open-loop (MAP) carrier estimation and closed-loop synchronization schemes to M-ary modulation schemes such as multiple phase-shift keying (MPSK) and quadrature amplitude-shift keying (QASK) also has been considered in the past [2,4,5].

Common to all of the above closed-loop schemes is the fact that the equivalent additive noise that perturbs the loop error signal can be modeled as a piecewise constant (over the duration of a data symbol, T_s) random process that is independent from symbol to symbol. Hence, the loop update likewise is independent from symbol to symbol, and the analysis of its performance can be determined by assuming

[1] Communications Systems and Research Section.

a triangular correlation function of width $2T_s$ for the equivalent additive noise. Also, the signal component of the loop error signal, i.e., the so-called S-curve, is a nonlinear (e.g., sinusoidal for low-SNR implementations) function of $M\phi_c$, with ϕ_c denoting the loop phase error, and as such the loop exhibits an M-fold phase ambiguity,

When the modulation is offset, such as for offset quadrature-phase-shift keying (OQPSK), both of the above observations become modified. First, the noise components in the I and Q channels corresponding to adjacent symbols overlap each other. Hence, the equivalent additive noise that perturbs the loop error signal, although still able to be modeled as a piecewise constant process, is no longer independent from symbol to symbol, i.e., adjacent symbol correlation exists. Second, the loop S-curve now need have only an 180-deg phase ambiguity (rather than the 90-deg phase ambiguity characteristic of QPSK carrier synchronization schemes) and as such resembles a BPSK carrier synchronization loop that tracks the 2ϕ process. This phenomenon was identified previously by Mengali [6, p. 232] for a decision-directed implementation of the OQPSK loop derived from MAP estimation considerations. Associated with this observation is the fact that, for OQPSK, the nonlinear loss that degrades the loop SNR will now be a *squaring loss* as opposed to the *fourth-power loss* typical of QPSK carrier synchronization loops.

In this article, we study the carrier synchronization problem for OQPSK in a more general framework than that considered in [6] in that we do not restrict ourselves to high-SNR (decision-directed) implementations of the MAP estimation loop. In particular, we explore in detail the noise and S-curve properties of the MAP estimation loop for OQPSK and their effect on its mean-square phase-error performance. We also present the behavior and performance of another OQPSK that has been implemented for future use in the Deep Space Network tracking stations [7]. This loop is an ad hoc but simple modification of that used for nonoffset QPSK and as such tracks the 4ϕ process with an accompanying 90-deg phase ambiguity. The performance of this suboptimal loop is compared with that of the true MAP estimation loop for OQPSK referred to above and found to be considerably inferior. In all cases, comparisons will be made on the basis of mean-squared phase jitter for equal loop bandwidths and signal-power-to-noise-power spectral density ratios. An equivalent comparison is in terms of the squaring loss[2] (the reduction in loop SNR relative to that of a phase-locked loop (PLL) of the same loop bandwidth).

II. Received Signal Model

For OQPSK, the I–Q carrier-modulated signal seen at the input to the receiver can be written in the form

$$s(t,\theta) = \sqrt{P}\left[m_I(t)\cos\left(\omega_c t + \theta\right) + m_Q(t)\sin\left(\omega_c t + \theta\right)\right] \tag{1}$$

where P is the signal power in watts and

$$\left.\begin{aligned} m_I(t) &= \sum_{n=-\infty}^{\infty} a_k p(t - kT_s) \\ m_Q(t) &= \sum_{n=-\infty}^{\infty} b_k p\left(t - \left(k + \frac{1}{2}\right)T_s\right) \end{aligned}\right\} \tag{2}$$

[2] Despite the fact that *squaring loss* is a term most appropriate to binary Costas loops, it nevertheless is used generically for loops corresponding to higher-order modulations such as QPSK even though in that instance *fourth-power loss* would be the more appropriate term.

with $\{a_k\}$ and $\{b_k\}$ respectively denoting the streams of independent, identically distributed (i.i.d.) binary (± 1) I and Q data symbols, T_s the symbol time, $p(t)$ a unit power rectangular pulse shape of duration T_s seconds and symmetric around $t = 0$, and θ the unknown carrier phase to be estimated. In addition to the signal in Eq. (1), the additive noise $n(t)$ present at the receiver input is characterized as a band-limited white Gaussian noise process with single-sided power spectral density N_0 W/Hz.

III. The MAP Estimation of Carrier Phase

Based on an observation of the received signal plus noise $x(t) = s(t, \theta) + n(t)$ over a time interval KT_s, we wish to estimate the random parameter θ (assumed to be time invariant over the observation interval) so as to maximize the a posteriori probability $p(\theta \,|x(t)\,)$.[3] Since the unknown phase θ can be assumed to be uniformly distributed in the interval $(-\pi, \pi)$, equivalently, we can maximize the conditional probability $p(x(t)\,|\theta\,)$. For the assumed additive white Gaussian noise channel model, the solution to this problem is well-known and can be obtained from the solution to the same problem corresponding to unbalanced QPSK (UQPSK) modulation [5]. In particular, since OQPSK is a special case of UQPSK corresponding to equal powers and equal data rates on both the I and Q channels as well as synchronous (but offset) I and Q data streams, then from [5, Eq. (14)], we immediately obtain an expression for the error signal $e(\phi)$ of the MAP estimation loop for OQPSK, namely,

$$e(\phi) = \sum_{k=1}^{K} \left[I_c(k, \phi) \tanh\{I_s(k, \phi)\} - I_s\left(k - \frac{1}{2}, \phi\right) \tanh\left\{ I_c\left(k - \frac{1}{2}, \phi\right)\right\}\right] \tag{3}$$

where

$$\left.\begin{aligned} I_s(k, \phi) &\triangleq \frac{2\sqrt{P}}{N_0} \int_{(k-1)T_s}^{kT_s} x(t) \sin\left(\omega_c t + \hat{\theta}\right) dt \\ I_c(k, \phi) &\triangleq \frac{2\sqrt{P}}{N_0} \int_{(k-1)T_s}^{kT_s} x(t) \cos\left(\omega_c t + \hat{\theta}\right) dt \end{aligned}\right\} \tag{4}$$

with $\hat{\theta}$ denoting the loop's estimate of the received carrier phase θ and $\phi \triangleq \theta - \hat{\theta}$ the associated loop phase error. For conventional (nonoffset) QPSK, the corresponding error signal to Eq. (3) would be

$$e(\phi) = \sum_{k=1}^{K} [I_c(k, \phi) \tanh\{I_s(k, \phi)\} - I_s(k, \phi) \tanh\{I_c(k, \phi)\}] \tag{5}$$

An implementation of a closed loop[4] based on Eq. (3) is illustrated in Fig. 1, where the K-symbol accumulator associated with the open-loop MAP estimate is replaced by a digital loop filter whose design is governed by the desired dynamic behavior of the loop.

---

[3] For convenience, we shall assume that K is integer, i.e., the observation interval corresponds to an integer number of baud intervals. This is typical of MAP estimation problems of this type.

[4] The illustration in Fig. 1 is slightly more generic in that it includes the possibility of a nonrectangular unit power T_s-second pulse shape, $p(t)$.

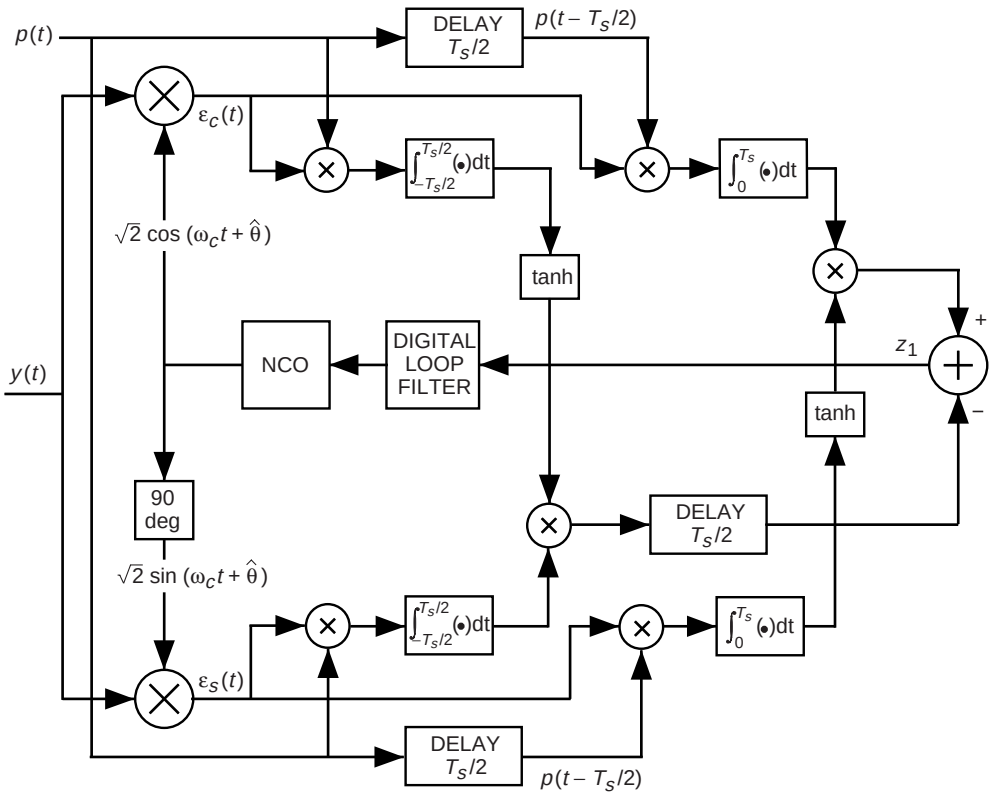

Fig. 1. Block diagram of the MAP carrier synchronization loop for offset pulse-shaped QPSK.

IV. Implementations for Low and High SNRs

As is customary in problems of this type, the hyperbolic tangent nonlinearity is replaced by its small and large argument approximations corresponding to small and large SNR applications. In the case of the latter, the appropriate approximation is $\tanh x \cong \text{sgn}\ x$, which results in a decision-directed implementation, e.g., [6, Fig. 5.23]. A tracking-performance analysis of this scheme for Nyquist channels and the assumption of perfect decisions [6, Eq. (5.25)] is given in [6, Section 5.4.2]. In the case of the former, the hyperbolic tangent function is approximated by the first or first two terms of its power series. For QPSK, if we use simply the approximation $\tanh x \cong x$ in Eq. (5), then the error signal $e(\phi)$ will degenerate to zero value for all ϕ and, hence, be of no use. Thus, for QPSK, we must use the first two terms of the power series, i.e., $\tanh x \cong x - x^3/3$, in which case the linear term still results in zero contribution to the error signal, but the cubic term gives [4]

$$e(\phi) = \sum_{k=1}^{K} I_c(k,\phi)\, I_s(k,\phi) \left[\left(I_c(k,\phi)\right)^2 - \left(I_s(k,\phi)\right)^2 \right] \tag{6}$$

which is of the form $IQ\left(Q^2 - I^2\right)$ and involves fourth-order product terms. Thus, as previously alluded to, in this instance the loop S-curve would be proportional to $\sin 4\phi$, and the squaring loss involves fourth-order noise product terms.

For OQPSK, using only the linear term of the hyperbolic tangent power series does not result in a degenerate error signal since applying the approximation $\tanh x \cong x$ to Eq. (3) results in

$$e(\phi) = \sum_{k=1}^{K} \left[I_c\left(k, \phi\right) I_s\left(k, \phi\right) - I_s\left(k - \frac{1}{2}, \phi\right) I_c\left(k - \frac{1}{2}, \phi\right) \right] \tag{7}$$

which has the form of the difference of two binary PSK error signals with a half symbol separation and, in general, is nonzero for arbitrary ϕ. Thus, since only second-order products are involved in Eq. (7), one would anticipate that the loop S-curve might be proportional to $\sin 2\phi$, and the squaring loss would involve only second-order noise product terms, as is the case for I–Q Costas loop tracking of BPSK. That such is the case is the subject of the tracking performance analysis to be presented in the next section.

A. Tracking-Performance Analysis of the Low SNR Implementation

In this section, we first derive the S-curve and equivalent noise of the I–Q loop of Fig. 1 (with a linear approximation to the hyperbolic tangent function) and then compute the loop's mean-square phase jitter. As previously mentioned, the signal $x(t)$ at the input to the receiver is composed of the sum of the signal $s\left(t, \theta\right)$ and a band-limited white Gaussian noise process that can be expressed in the form

$$n(t) = \sqrt{2}\left[N_c(t)\cos\left(\omega_c t + \theta\right) - N_s(t)\sin\left(\omega_c t + \theta\right)\right] \tag{8}$$

where $N_c(t)$ and $N_s(t)$ are independent low-pass white Gaussian noise processes with single-sided power spectral density N_0 W/Hz. Demodulating $x(t)$ with the quadrature reference signals $r_c(t) = \sqrt{2}\cos\left(\omega_c t + \hat{\theta}\right)$ and $r_s(t) = \sqrt{2}\sin\left(\omega_c t + \hat{\theta}\right)$ produces (ignoring second-order harmonics of the carrier) the quadrature phase detector outputs

$$\left.\begin{aligned} \varepsilon_c(t) &= \left[\sqrt{\frac{P}{2}} m_Q(t) - N_s(t)\right]\sin\phi + \left[\sqrt{\frac{P}{2}} m_I(t) + N_c(t)\right]\cos\phi \\ \varepsilon_s(t) &= \left[\sqrt{\frac{P}{2}} m_Q(t) - N_s(t)\right]\cos\phi - \left[\sqrt{\frac{P}{2}} m_I(t) + N_c(t)\right]\sin\phi \end{aligned}\right\} \tag{9}$$

where $\phi \triangleq \theta - \hat{\theta}$ denotes the phase error in the loop. Integrating over the appropriate time intervals corresponding to the transmitted I and Q symbols[5] gives the pairs of signals $z_c(t), z_s(t)$ and $z_c'(t), z_s'(t)$, which are used to form the loop-error signal. Assuming a modulation $m(t)$ as in Eq. (1), these signals take the form[6]

$$\left.\begin{aligned} z_c(t) &= \int_{-T_s/2}^{T_s/2} \varepsilon_c(t)dt = \left[\sqrt{\frac{P}{2}} T_s \frac{b_0 + b_{-1}}{2} - N_1\right]\sin\phi + \left[\sqrt{\frac{P}{2}} T_s a_0 + N_2\right]\cos\phi \\ z_s(t) &= \int_{-T_s/2}^{T_s/2} \varepsilon_s(t)dt = \left[\sqrt{\frac{P}{2}} T_s \frac{b_0 + b_{-1}}{2} - N_1\right]\cos\phi - \left[\sqrt{\frac{P}{2}} T_s a_0 + N_2\right]\sin\phi, \quad \frac{T_s}{2} \le t \le \frac{3T_s}{2} \end{aligned}\right\} \tag{10a}$$

and

[5] For convenience, we assume the first ($k = 1$) baud interval for the I and Q integrate-and-dump (I&D) filters corresponding to the transmitted symbols a_0 and b_0.

[6] We can ignore the weighting of the integrators by the factor $2\sqrt{P}/N_0$ since, for this implementation, this gain eventually will be absorbed in the total loop gain. As such, $z_c(t), z_s(t), z_c'(t)$, and $z_s'(t)$ are normalized versions of $I_c(k,\theta), I_s(k,\theta), I_c'(k,\theta)$, and $I_s'(k,\theta)$ corresponding to $k = 1$.

$$\left.\begin{aligned} z_c'(t) &= \int_0^{T_s} \varepsilon_c(t)dt = \left[\sqrt{\frac{P}{2}}T_s b_0 - N_1'\right]\sin\phi + \left[\sqrt{\frac{P}{2}}T_s\frac{a_0+a_1}{2} + N_2'\right]\cos\phi \\ z_s'(t) &= \int_0^{T_s} \varepsilon_s(t)dt = \left[\sqrt{\frac{P}{2}}T_s b_0 - N_1'\right]\cos\phi - \left[\sqrt{\frac{P}{2}}T_s\frac{a_0+a_1}{2} + N_2'\right]\sin\phi, \quad T_s \le t \le 2T_s \end{aligned}\right\} \tag{10b}$$

where N_1, N_2, N_1', and N_2' are zero-mean Gaussian random variables defined by

$$\left.\begin{aligned} N_1 &\triangleq \int_{-T_s/2}^{T_s/2} N_s(t)dt \\ N_2 &\triangleq \int_{-T_s/2}^{T_s/2} N_c(t)dt \\ N_1' &\triangleq \int_0^{T_s} N_s(t)dt \\ N_2' &\triangleq \int_0^{T_s} N_c(t)dt \end{aligned}\right\} \tag{11}$$

all with variance $\sigma_N^2 = N_0T_s/2$. Although N_1 and N_2 are uncorrelated, and likewise for N_1' and N_2', because of the offset between the I and Q channels, the pairs N_1, N_1', and N_2, N_2' are indeed correlated with

$$E\{N_1N_1'\} = E\{N_2N_2'\} = \frac{N_0T_s}{4} \tag{12}$$

However, the pairs N_1N_2' and $N_1'N_2$ are still uncorrelated.

Multiplying $z_c'(t)$ and $z_s'(t)$ and subtracting the product of $z_c(t-T_s/2)$ and $z_s(t-T_s/2)$ produces the error signal corresponding to the first baud interval in accordance with Eq. (7), namely,

$$\begin{aligned} z_1(t) &= z_c'(t)z_s'(t) - z_c\left(\frac{t-T_s}{2}\right)z_s\left(\frac{t-T_s}{2}\right) \\ &= \frac{1}{4}PT_s^2\left[b_0^2 + a_0^2 - \left(\frac{a_0+a_1}{2}\right)^2 - \left(\frac{b_0+b_{-1}}{2}\right)^2\right]\sin 2\phi \\ &\quad + \frac{1}{2}PT_s^2\left[b_0\left(\frac{a_0+a_1}{2}\right) - a_0\left(\frac{b_0+b_{-1}}{2}\right)\right]\cos 2\phi - \frac{N_e(t,2\phi)}{2} \\ &= \frac{1}{4}PT_s^2\left\{\left[1 - \frac{a_0a_1}{2} - \frac{b_0b_1}{2}\right]\sin 2\phi + [b_0(a_0+a_1) - a_0(b_0+b_1)]\cos 2\phi\right\} - \frac{N_e(t,2\phi)}{2}, \\ &\qquad\qquad T_s \le t \le 2T_s \end{aligned} \tag{13}$$

where the first two (signal) terms account for the signal × signal products and $N_e(t, 2\phi)$ is an equivalent noise (as if it appeared at the loop input) that accounts for the remaining signal × noise and noise × noise products that, after some simplification, becomes

$$N_e(t, 2\phi) = \sin 2\phi$$

$$\times \left\{ -\left(N_1'\right)^2 + \left(N_2'\right)^2 - N_2^2 + N_1^2 - \sqrt{\frac{P}{2}} T_s \left[\left(b_0 + b_{-1}\right) N_1 - 2b_0 N_1' - \left(a_0 + a_1\right) N_2' + 2a_0 N_2 \right] \right\}$$

$$+ \cos 2\phi \left\{ 2N_1' N_2' - 2N_1 N_2 - \sqrt{\frac{P}{2}} T_s \left[2b_0 N_2' + 2a_0 N_1 - \left(b_0 + b_{-1}\right) N_2 - \left(a_0 + a_1\right) N_1' \right] \right\},$$

$$T_s \le t \le 2T_s \tag{14}$$

and is a piecewise constant (over intervals of T_s seconds) random process.

The statistical mean (over the data symbols) of the signal term represents the loop S-curve. Thus, averaging the signal terms of Eq. (13) over the data gives

$$\overline{z_1(t)} \triangleq \frac{1}{2} S(\phi) = \frac{1}{2} \left(\frac{1}{2} P T_s^2 \sin 2\phi \right) \triangleq \frac{1}{2} K_g \sin 2\phi \tag{15}$$

as previously anticipated, where $K_g = PT_s^2/2$ denotes the slope (with respect to the 2ϕ process) of the S-curve $S(\phi)$ at the origin. The difference between the signal components of $z_1(t)$ and their mean represents self-modulation noise that, at very large symbol SNR $E_s/N_0 = PT_s/N_0$ produces an error floor in the loop mean-square phase-error performance [6]. For the purpose of the analysis here, we shall ignore this self-noise since, in the typical region of symbol SNRs of interest (below about 15 dB), it has negligible influence on the performance. If necessary, evaluation of the self-noise can be carried out in an analogous fashion to that considered in [2,6].

Linearizing the loop (i.e., replacing $\sin 2\phi$ by 2ϕ), as is appropriate in the typical operating region of large loop SNRs, then following the approach in [2], the mean-square error of the 2ϕ process can be computed from

$$\sigma_{2\phi}^2 = \frac{N_E B_L}{K_g^2} \tag{16}$$

where B_L denotes the loop bandwidth and N_E is the flat single-sided power spectral density of the equivalent noise process[7] $N_e(t, 0)$, which can be modeled as a delta-correlated process [2] with autocorrelation function $R_{N_e}(\tau) = E\{N_e(t, 0) N_e(t + \tau, 0)\}$. Thus,

$$N_E = 2 \int_{-\infty}^{\infty} R_{N_e}(\tau) d\tau \tag{17}$$

[7] In the linear region of loop operation, we can, without loss of generality, assume $\phi = 0$ in so far as the noise power evaluation is concerned.

The mean-square phase error of Eq. (16) can be rewritten in the form

$$\left.\begin{aligned} \sigma_{2\phi}^2 &= \frac{4}{\rho S_L} \\ \rho &\triangleq \frac{P}{N_0 B_L} \\ S_L &\triangleq 4\left(\frac{K_g^2/P}{N_E/N_0}\right) \end{aligned}\right\} \tag{18}$$

where ρ is the loop SNR of an equivalent linear loop (e.g., the PLL) and S_L is the so-called squaring loss, as previously mentioned. We now proceed to evaluate the equivalent power spectral density N_E defined in Eq. (17).

From Eq. (14), we have that

$$\begin{aligned} N_e(t,0) &= 2N_1'(1)\,N_2'(1) - 2N_1(1)\,N_2(1) \\ &\quad - \sqrt{\frac{P}{2}}T_s\left[2b_0N_2'(1) + 2a_0N_1(1) - (b_0+b_{-1})\,N_2(1) - (a_0+a_1)\,N_1'(1)\right], \\ &\qquad\qquad T_s \le t \le 2T_s \end{aligned} \tag{19}$$

where we have introduced the parenthetical notation "(1)" to the integrated noise variables to relate to the fact that, as per their definition in Eq. (11), they correspond to the first ($k = 1$) baud interval. For the following baud interval, the analogous expression to Eq. (19) would be

$$\begin{aligned} N_e(t,0) &= 2N_1'(2)\,N_2'(2) - 2N_1(2)\,N_2(2) \\ &\quad - \sqrt{\frac{P}{2}}T_s\left[2b_1N_2'(2) + 2a_1N_1(2) - (b_1+b_0)\,N_2(2) - (a_1+a_2)\,N_1'(2)\right], \\ &\qquad\qquad 2T_s \le t \le 3T_s \end{aligned} \tag{20}$$

where, in accordance with Eq. (11), $N_1(2)$ and $N_2(2)$ are the quadrature noise components integrated over the interval $T_s/2 \le t \le 3T_s/2$ and $N_1'(2)$ and $N_2'(2)$ are the analogous components integrated over the interval $T_s \le t \le 2T_s$. Clearly, the equivalent noises in Eqs. (19) and (20) are correlated because of the overlap of the unprimed and primed noise components brought about by the offset in the I and Q integration intervals.[8] This phenomenon is different from that for nonoffset QPSK, where the equivalent noise components are uncorrelated from symbol interval to symbol interval. Because of this adjacent symbol noise correlation, the correlation function of $N_e(t,0)$ is piecewise linear over a time interval $-2T_s \le t \le 2T_s$, as illustrated in Fig. 2 and, hence, it is sufficient to compute the values of $R_{N_e}(\tau)$

[8] This correlation extends only into adjacent symbol intervals since beyond that the integration intervals for the unprimed and primed noise components do not overlap.

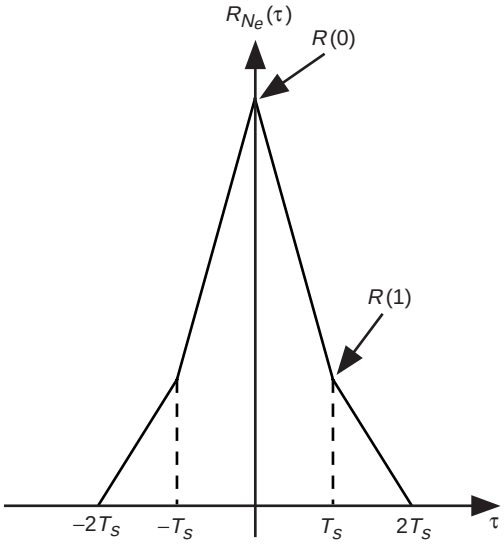

Fig. 2. The autocorrelation function of the equivalent noise process.

at integer multiples of T_s, namely, $R_{N_e}(nT_s) \triangleq R(n)$, where $R(0) = E\left\{N_e^2(t,0)\right\} = \sigma_{N_e}^2$. Furthermore, since $R_{N_e}(\tau)$ extends only from $-2T_s$ to $2T_s$, then in view of Eq. (17), the equivalent noise spectral density is given by

$$N_E = 2T_s\left[R(0) + 2R(1)\right] \tag{21}$$

Evaluation of $R(0)$ and $R(1)$ can be obtained from the variance of Eq. (19) and the cross-correlation of Eqs. (19) and (20), respectively. In particular,

$$R(0) = 4E\left\{\left(N_1'(1)\,N_2'(1) - N_1(1)\,N_2(1)\right)^2\right\}$$

$$+ 2PT_s^2 E\left\{\left(b_0 N_2'(1) + a_0 N_1(1) - \left(\frac{b_0+b_{-1}}{2}\right)N_2(1) - \left(\frac{a_0+a_1}{2}\right)N_1'(1)\right)^2\right\} \tag{22}$$

where the expectation is over both the noise components and the data symbols. Making use of the equal variance of the noise components, i.e., $\sigma_N^2 = N_0T_s/2$, and their correlation property of Eq. (12), the autocorrelation in Eq. (22) becomes, after simplification (see Appendix A),

$$R(0) = \frac{3}{2}N_0^2T_s^2\left(1 + \frac{4}{3}\frac{PT_s}{N_0}\right) \tag{23}$$

Similarly,

$$R(1) = 4E\left\{\left(N_1'(1)\,N_2'(1) - N_1(1)\,N_2(1)\right)\left(N_1'(2)\,N_2'(2) - N_1(2)\,N_2(2)\right)\right\}$$

$$+ 2PT_s^2 E\left\{\left(b_0 N_2'(1) + a_0 N_1(1) - \left(\frac{b_0+b_{-1}}{2}\right)N_2(1) - \left(\frac{a_0+a_1}{2}\right)N_1'(1)\right)\right.$$

$$\left.\times\left(b_1 N_2'(2) + a_1 N_1(2) - \left(\frac{b_1+b_0}{2}\right)N_2(2) - \left(\frac{a_1+a_2}{2}\right)N_1'(2)\right)\right\} \tag{24}$$

which after simplification becomes

$$R(1) = -\frac{1}{4}N_0^2 T_s^2 \left(1 + 2\frac{PT_s}{N_0}\right) \tag{25}$$

Substituting Eqs. (23) and (25) in Eq. (21) gives

$$\frac{N_E}{N_0} = 2N_0 T_s^3 \left(1 + \frac{PT_s}{N_0}\right) \tag{26}$$

Finally, using Eq. (26) and the S-curve slope from Eq. (15) in Eq. (18), we obtain the desired result for the squaring loss, namely,

$$S_L = \frac{1}{2}\left(\frac{E_s/N_0}{1 + E_s/N_0}\right) \tag{27a}$$

or, in terms of the bit-energy-to-noise ratio, $E_b/N_0 = E_s/2N_0$,

$$S_L = \frac{1}{2}\left(\frac{2E_b/N_0}{1 + 2E_b/N_0}\right) \tag{27b}$$

which interestingly enough is one-half the result for a Costas I–Q loop-tracking BPSK modulation of the same bit rate [2, Eq. (73)]. The analogous result to Eq. (27b) for the low-SNR implementation of the MAP carrier-synchronization loop for nonoffset QPSK is given by [8, Eq. (3.3-58)]:

$$S_L = \frac{1}{1 + \dfrac{9}{4E_b/N_0} + \dfrac{3}{2\left(E_b/N_0\right)^2} + \dfrac{3}{16\left(E_b/N_0\right)^3}} \tag{28}$$

B. Tracking Performance Analysis of the High-SNR Implementation

In this section, we first derive the S-curve and equivalent noise of the I–Q loop of Fig. 1 (with a hard limiter approximation to the hyperbolic tangent function) and then compute the loop's mean-square phase jitter. Analogous to Eq. (13), the loop-error signal is now

$$z_1(t) = z_c'(t)\ \text{sgn}\ z_s'(t) - z_s\left(\frac{t - T_s}{2}\right)\ \text{sgn}\ z_c\left(\frac{t - T_s}{2}\right), \quad T_s \le t \le 2T_s \tag{29}$$

where $z_s(t)z_c(t)$ and $z_c'(t), z_s'(t)$ are as defined in Eqs. (10a) and (10b), respectively. Substituting Eq. (10) in Eq. (29) and averaging over the noise and data symbols, we obtain after considerable evaluation (see Appendix B)

$$\overline{z_1(t)} \triangleq \frac{1}{2}S(\phi) = \frac{1}{2}\sqrt{\frac{P}{2}}T_s\left[(\sin\phi-\cos\phi)\ \mathrm{erf}\left(\sqrt{\frac{E_s}{2N_0}}(\cos\phi+\sin\phi)\right)\right.$$

$$\left.+(\sin\phi+\cos\phi)\ \mathrm{erf}\left(\sqrt{\frac{E_s}{2N_0}}(\cos\phi-\sin\phi)\right)+2\sin\phi\,\mathrm{erf}\left(\sqrt{\frac{E_s}{2N_0}}\cos\phi\right)\right] \quad (30)$$

where $\mathrm{erf}(x) \triangleq 2/\sqrt{\pi}\int_0^x \exp\left(-y^2/2\right)dy$ is the error function. Note that $S(\phi) = S(\phi \pm \pi)$ and, thus, once again the S-curve is periodic with period π, i.e., the loop tracks a 2ϕ (rather than 4ϕ) process. Figure 3 is a plot of the normalized S-curve [the quantity in brackets in Eq. (30)] with bit SNR $E_b/N_0 = E_s/2N_0$ as a parameter. In the limit of infinite SNR, the S-curve behaves as

$$S(\phi) = \sqrt{\frac{P}{2}}T_s\left[(\sin\phi-\cos\phi)\,\mathrm{sgn}\ (\cos\phi+\sin\phi)+(\sin\phi+\cos\phi)\,\mathrm{sgn}\ (\cos\phi-\sin\phi)+2\sin\phi\,\mathrm{sgn}\ (\cos\phi)\right] \quad (31a)$$

or equivalently

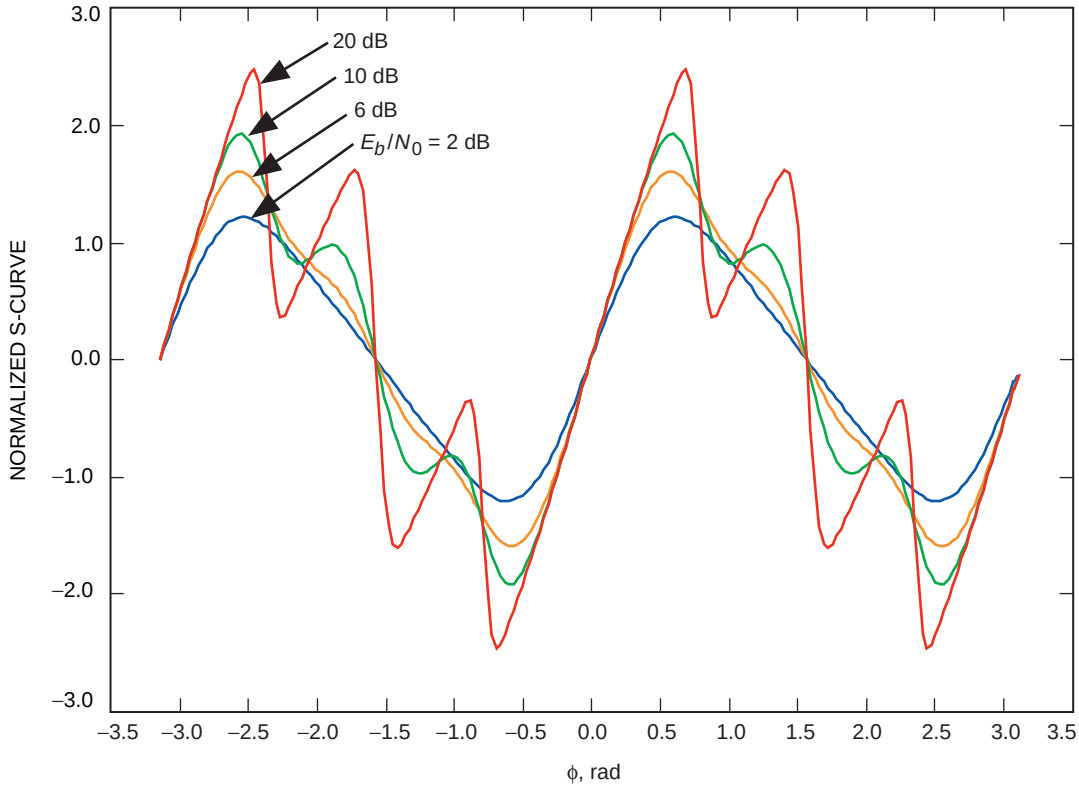

Fig. 3. Normalized S-curves for the high SNR implementation of the MAP carrier synchronization loop for OQPSK.

$$S(\phi) = \sqrt{\frac{P}{2}} T_s \begin{cases} 4\sin\phi, & 0 \le \phi \le \dfrac{\pi}{4} \\ 2(\sin\phi - \cos\phi), & \dfrac{\pi}{4} \le \phi \le \dfrac{\pi}{2} \\ 2(-\sin\phi - \cos\phi), & \dfrac{\pi}{2} \le \phi \le \dfrac{3\pi}{4} \\ -4\sin\phi, & \dfrac{3\pi}{4} \le \phi \le \pi \end{cases} \tag{31b}$$

Comparing Fig. 3 with the qualitative version of the S-curve as given in [6, Fig. 5.24], we see that the latter, which is reasoned on the basis that $S(\phi) \approx \sin\phi$ in the neighborhood of small ϕ and $S(\pi/2) = 0$ (both of which are true), is indicative of the true behavior only at a small SNR. At a large SNR, which is the assumption made in [6] (i.e., the data decisions are assumed to be perfect), the S-curve has a somewhat different behavior, as can be seen in Fig. 3. The slope of the S-curve in Eq. (30) at the origin is obtained as

$$K_g \triangleq \frac{dS(\phi)}{d(2\phi)} = \frac{1}{2}\frac{dS(\phi)}{d\phi} = 2\sqrt{\frac{P}{2}} T_s \left[\operatorname{erf}\left(\sqrt{\frac{E_s}{2N_0}} \right) - \sqrt{\frac{E_s}{2N_0\pi}} \exp\left(-\frac{E_s}{2N_0} \right) \right] \tag{32}$$

and will be used shortly in determining the squaring loss.

The equivalent additive noise component at the loop input, which is related to the noise component of the error signal by $N_e(t, 2\phi)/2 = -\left(z_1(t) - \overline{z_1(t)}\right)$, is obtained by subtracting Eq. (30) from Eq. (29). When evaluated at $\phi = 0$, this equivalent noise becomes

$$\begin{aligned} N_e(t,0) = &-2\left[\sqrt{\frac{P}{2}} T_s \frac{a_0 + a_1}{2} + N_2'(1) \right] \operatorname{sgn}\left[\sqrt{\frac{P}{2}} T_s b_0 - N_1'(1) \right] \\ &+ 2\left[\sqrt{\frac{P}{2}} T_s \frac{b_0 + b_{-1}}{2} - N_1(1) \right] \operatorname{sgn}\left[\sqrt{\frac{P}{2}} T_s a_0 + N_2(1) \right], \\ &\qquad T_s \le t \le 2T_s \end{aligned} \tag{33a}$$

and

$$\begin{aligned} N_e(t,0) = &-2\left[\sqrt{\frac{P}{2}} T_s \frac{a_1 + a_2}{2} + N_2'(2) \right] \operatorname{sgn}\left[\sqrt{\frac{P}{2}} T_s b_1 - N_1'(2) \right] \\ &+ 2\left[\sqrt{\frac{P}{2}} T_s \frac{b_1 + b_0}{2} - N_1(2) \right] \operatorname{sgn}\left[\sqrt{\frac{P}{2}} T_s a_1 + N_2(2) \right], \\ &\qquad 2T_s \le t \le 3T_s \end{aligned} \tag{33b}$$

where again we have introduced the parenthetical notation "(k)" to correspond to the kth ($k = 1, 2$) baud integration interval of the quadrature noise components. Once again we must determine the variance and

correlation coefficients of $N_e(t,0)$ in order to determine its equivalent noise power spectral density. The details of these evaluations are quite lengthy and are presented in Appendix C. The final results are

$$\left.\begin{aligned} R(0) &= E\left\{N_e^2(t,0)\right\} = 4N_0T_s\left(1+\frac{E_s}{2N_0}-\left[\sqrt{\frac{E_s}{4N_0}}\operatorname{erf}\sqrt{\frac{E_s}{2N_0}}+\frac{1}{\sqrt{2\pi}}\exp\left(-\frac{E_s}{2N_0}\right)\right]^2\right) \\ R(1) &= E\left\{N_e(t,0)N_e(t+T_s,0)\right\} = -2N_0T_s\left[\sqrt{\frac{E_s}{4N_0}}\operatorname{erf}\sqrt{\frac{E_s}{2N_0}}+\frac{1}{\sqrt{2\pi}}\exp\left(-\frac{E_s}{2N_0}\right)\right]^2 \end{aligned}\right\} \tag{34}$$

Substituting Eq. (34) into Eq. (21), we obtain the single-sided power spectral density of the equivalent noise as

$$N_E = 8N_0T_s^2\left(1+\frac{E_s}{2N_0}-\left[\sqrt{\frac{E_s}{2N_0}}\operatorname{erf}\sqrt{\frac{E_s}{2N_0}}+\frac{1}{\sqrt{\pi}}\exp\left(-\frac{E_s}{2N_0}\right)\right]^2\right) \tag{35}$$

Finally, substituting Eqs. (32) and (35) in Eq. (18) and substituting E_b/N_0 for $E_s/2N_0$, the squaring loss of the high SNR implementation of the MAP carrier synchronization loop for OQPSK becomes

$$S_L = \frac{\left[\operatorname{erf}\left(\sqrt{\frac{E_b}{N_0}}\right)-\sqrt{\frac{E_b}{N_0\pi}}\exp\left(-\frac{E_b}{N_0}\right)\right]^2}{1+\frac{E_b}{N_0}-\left[\sqrt{\frac{E_b}{N_0}}\operatorname{erf}\sqrt{\frac{E_b}{N_0}}+\frac{1}{\sqrt{\pi}}\exp\left(-\frac{E_b}{N_0}\right)\right]^2} \tag{36}$$

The analogous result to Eq. (36) for the high SNR implementation of the MAP carrier synchronization loop for nonoffset QPSK is given by [9, Eq. (3.3-57)]:

$$S_L = \frac{\left[\operatorname{erf}\left(\sqrt{\frac{E_b}{N_0}}\right)-2\sqrt{\frac{E_b}{N_0\pi}}\exp\left(-\frac{E_b}{N_0}\right)\right]^2}{1+\frac{2E_b}{N_0}-2\left[\sqrt{\frac{E_b}{N_0}}\operatorname{erf}\sqrt{\frac{E_b}{N_0}}+\frac{1}{\sqrt{\pi}}\exp\left(-\frac{E_b}{N_0}\right)\right]^2} \tag{37}$$

Figure 4 is a plot of the squaring loss versus E_b/N_0 in dB for the various loop implementations considered above. We observe that at a low bit SNR (where the squaring loss is significant), the OQPSK implementations have a decided advantage over their QPSK counterparts. Also, the crossover point below which the low SNR approximation of the OQPSK loop outperforms the high SNR approximation is -2.5 dB.

V. A Suboptimum Implementation Derived From the MAP Implementation for QPSK

Another (albeit ad hoc) implementation of a carrier synchronization loop for OQPSK was initially proposed for the design of the Advanced Receiver II (ARX II) [7] and is now included in the Block V receiver in NASA's Deep Space Network (DSN) [8]. This scheme, which is illustrated in Fig. 5(a), merely delays the quadrature arm so as to align it with the in-phase arm and then proceeds to process the

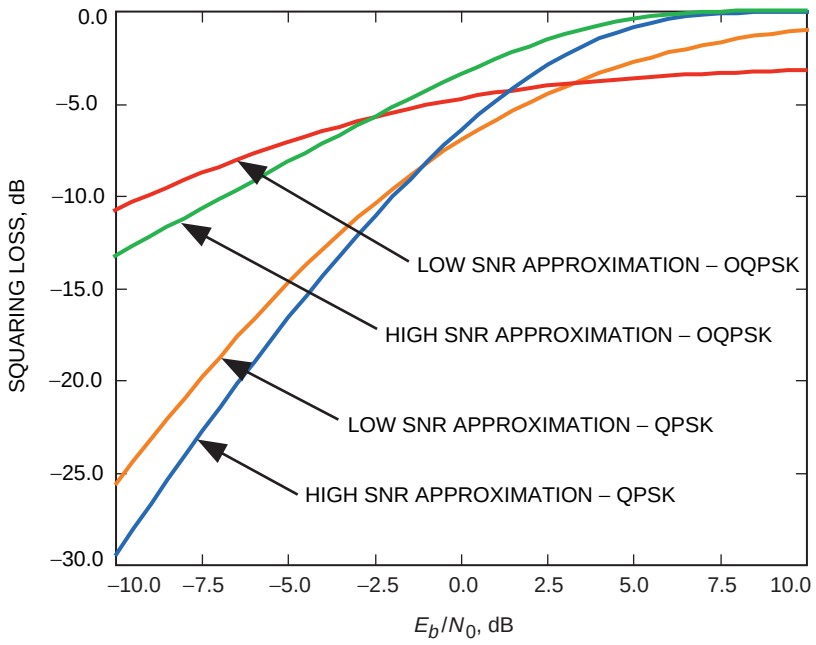

Fig. 4. Squaring loss performance comparison of various MAP carrier synchronization loop implementations.

I and Q signals as one would do in the MAP implementation of nonoffset QPSK.[9] Ignoring the MAP estimation approach, such a scheme could be argued to be intuitively logical in view of the manner in which the data symbols of OQPSK traditionally are detected. Note that this implementation forms its $I \tanh Q$ and $Q \tanh I$ from the same pair of I and Q signals and, thus, a low SNR implementation would require the first two terms in the power series expansion of the hyperbolic tangent function, i.e., a fourth-order loop that tracks the 4ϕ process with an error signal akin to Eq. (5). An illustration of such a low SNR implementation is shown in Fig. 5(b). It is interesting to investigate how suboptimal (from the standpoint of squaring loss) this implementation is relative to that obtained by linearizing the hyperbolic tangent function in Fig. 1 as analyzed in Section IV.

Analogous to Eq. (10a), the I and Q integrate-and-dump outputs in Fig. 5(b) are given by

$$\left.\begin{aligned} z_c(t) &= \int_{-T_s/2}^{T_s/2} \varepsilon_c(t)dt = \left[\sqrt{\frac{P}{2}}T_s\frac{b_0+b_{-1}}{2} - N_1\right]\sin\phi + \left[\sqrt{\frac{P}{2}}T_s a_0 + N_2\right]\cos\phi \\ z_s(t) &= \int_{-T_s/2}^{T_s/2} \varepsilon_s\left(t-\frac{T_s}{2}\right)dt = \left[\sqrt{\frac{P}{2}}T_s b_{-1} - N_1'\right]\cos\phi - \left[\sqrt{\frac{P}{2}}T_s\frac{a_0+a_{-1}}{2} + N_2'\right]\sin\phi, \\ &\qquad\qquad \frac{T_s}{2} \le t \le \frac{3T_s}{2} \end{aligned}\right\} \quad (38)$$

where N_1, N_2, N_1', and N_2' are zero-mean Gaussian random variables that now are defined by

[9] In the actual receiver design, the delay and I&D filter in the I arm are actually reversed and, likewise, the range of the I&D filter in the Q arm extends from 0 to T_s. However, this is of no consequence to the performance analysis that follows.

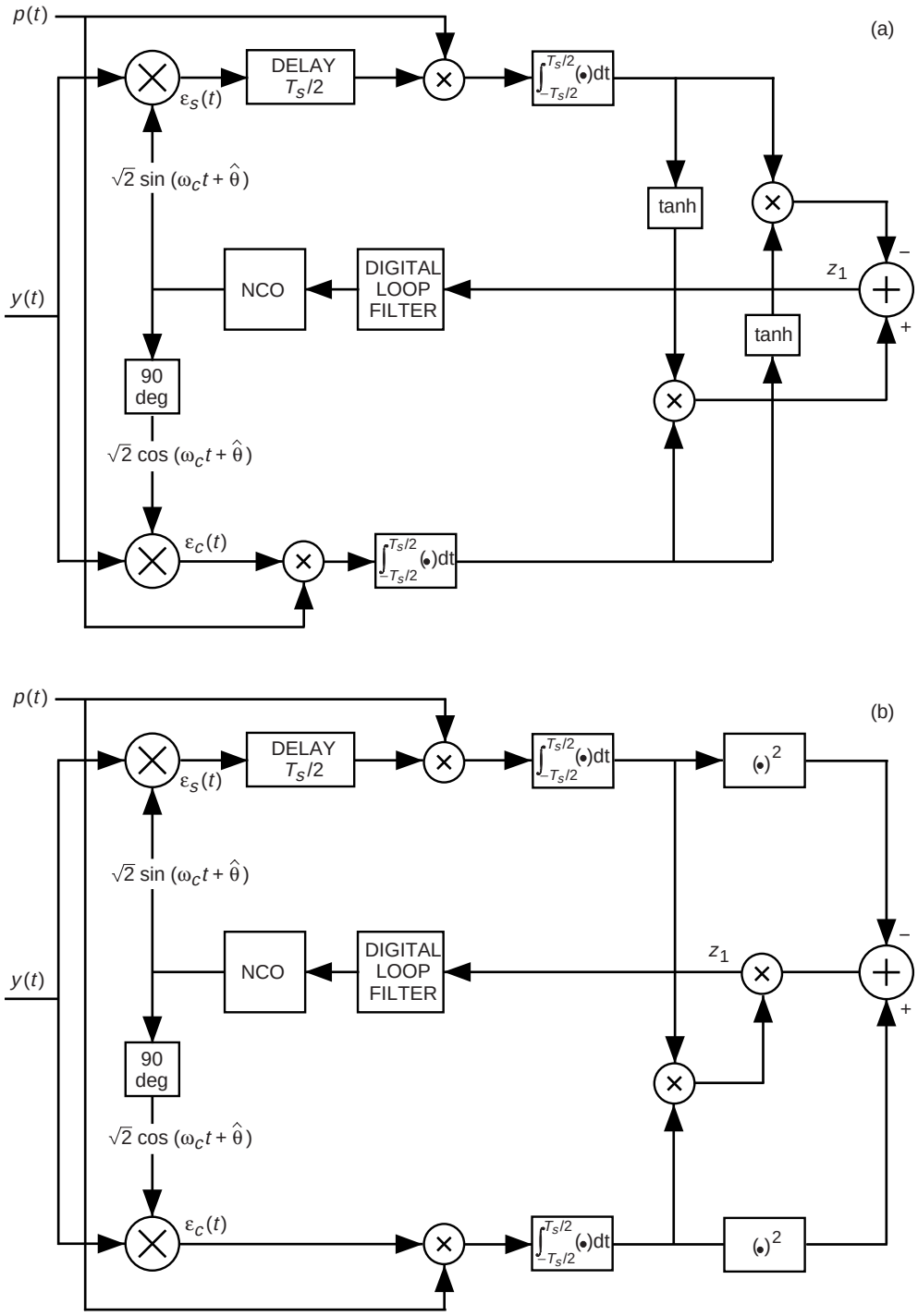

Fig. 5. Offset pulse-shaped QPSK with QPSK post-detection processing: (a) the suboptimum carrier synchronization loop and (b) the low SNR implementation of the suboptimum carrier synchronization loop.

$$\left.\begin{aligned} N_1 &\triangleq \int_{-T_s/2}^{T_s/2} N_s(t)dt \\ N_2 &\triangleq \int_{-T_s/2}^{T_s/2} N_c(t)dt \\ N_1' &\triangleq \int_{-T_s/2}^{T_s/2} N_s\left(t-\frac{T_s}{2}\right)dt = \int_{-T_s}^{0} N_s(t)dt \\ N_2' &\triangleq \int_{-T_s/2}^{T_s/2} N_c\left(t-\frac{T_s}{2}\right)dt = \int_{-T_s}^{0} N_c(t)dt \end{aligned}\right\} \tag{39}$$

all with variance $\sigma_N^2 = N_0 T_s/2$. Once again N_1 and N_2 are uncorrelated, and likewise for N_1' and N_2', but because of the offset between the I and Q channels, the pairs N_1, N_1' and N_2, N_2' are indeed correlated, with the correlation given by Eq. (12). The pairs $N_1 N_2'$ and $N_1' N_2$ are, however, still uncorrelated.

The error signal analogous to Eq. (13) is obtained from Fig. 5(b) as

$$z_1(t) = z_c(t) z_s(t) \left[z_c^2(t) - z_s^2(t)\right] \tag{40}$$

Substituting Eq. (38) into Eq. (40) and simplifying the algebra and trigonometry, the signal component of Eq. (40), i.e., the statistical mean with respect to the noise components, is given by

$$\begin{aligned} E_N\left\{z_1(t)\right\} = \frac{1}{4}P^2T_s^4 \Bigg\{ & \frac{1}{2}\left[b_{-1}\left(\frac{b_{-1}+b_0}{2}\right) - a_0\left(\frac{a_{-1}+a_0}{2}\right)\right]\sin 2\phi + a_0 b_{-1}\cos^2\phi \\ & + \left(\frac{a_{-1}+a_0}{2}\right)\left(\frac{b_{-1}+b_0}{2}\right)\sin^2\phi \Bigg\} \\ & \times \Bigg\{ \left[a_0\left(\frac{b_{-1}+b_0}{2}\right) - b_{-1}\left(\frac{a_{-1}+a_0}{2}\right)\right]\sin 2\phi + \left(a_0^2 - b_{-1}^2\right)\cos^2\phi \\ & + \left[\left(\frac{b_{-1}+b_0}{2}\right)^2 - \left(\frac{a_{-1}+a_0}{2}\right)^2\right]\sin^2\phi \Bigg\} \end{aligned} \tag{41}$$

Statistically averaging Eq. (41) over the data symbols results, after much simplification, in

$$\begin{aligned} \overline{z_1(t)} \triangleq \frac{1}{4}S\left(\phi\right) &= \frac{1}{4}P^2T_s^4 \sin 2\phi \left(\cos^2\phi - \frac{1}{4}\sin^2\phi\right) \\ &= \frac{1}{4}P^2T_s^4 \left(\frac{3}{8}\sin 2\phi + \frac{5}{16}\sin 4\phi\right) \end{aligned} \tag{42}$$

As predicted, the S-curve $S(\phi)$ in Eq. (42) is periodic with period $\pi/2$ and, hence, the loop tracks the 4ϕ process. The slope of the S-curve at the origin, K_g, is obtained by evaluating the derivative of $S(\phi)$ with respect to 4ϕ at $\phi = 0$, with the result

$$K_g = \frac{1}{2}P^2T_s^4 \tag{43}$$

The noise component of the error signal evaluated at $\phi = 0$ is obtained from Eqs. (38) and (40) as

$$\begin{aligned} -\frac{N_e(t,0)}{4} &= \overline{z_1(t)}\,|_{\phi=0} \\ &= \left(\sqrt{\frac{P}{2}}T_s b_{-1} - N_1'\right)\left(\sqrt{\frac{P}{2}}T_s a_0 + N_2\right)\left[\left(\sqrt{\frac{P}{2}}T_s a_0 + N_2\right)^2 - \left(\sqrt{\frac{P}{2}}T_s b_{-1} - N_1'\right)^2\right] \end{aligned} \tag{44}$$

Evaluation of the correlation function of $N_e(t,0)$ for values of τ corresponding to integer multiples of T_s proceeds as in Appendix A but now involves fourth-order signal $\times$ noise and noise $\times$ noise moments. The details are presented in Appendix D, where the following results are obtained:

$$\left.\begin{aligned} R(0) &= E\left\{(N_e(t,0))^2\right\} = 8\left[P^3N_0T_s^7 + \frac{9}{2}P^2N_0^2T_s^6 + 6PN_0^3T_s^5 + \frac{3}{2}N_0^4T_s^4\right] \\ &= 8P^3N_0T_s^7\left[1 + \frac{9}{2E_s/N_0} + \frac{6}{(E_s/N_0)^2} + \frac{3}{2(E_s/N_0)^3}\right] \\ R(1) &= 0 \end{aligned}\right\} \tag{45}$$

and, thus, from Eq. (21) the equivalent noise power spectral density normalized by N_0 is

$$\frac{N_E}{N_0} = 16P^3T_s^8\left[1 + \frac{9}{2E_s/N_0} + \frac{6}{(E_s/N_0)^2} + \frac{3}{2(E_s/N_0)^3}\right] \tag{46}$$

Since the loop now tracks a 4ϕ process, the mean-square error of this process can be written, analogous to Eq. (18), as

$$\left.\begin{aligned} \sigma_{4\phi}^2 &= \frac{16}{\rho S_L} \\ \rho &\triangleq \frac{P}{N_0B_L} \\ S_L &\triangleq 16\left(\frac{K_g^2/P}{N_E/N_0}\right) \end{aligned}\right\} \tag{47}$$

Finally, substituting Eqs. (43) and (46) in Eq. (47) gives the desired result for the squaring loss, namely,

$$S_L = \frac{1}{4}\left[\frac{1}{1+\dfrac{9}{2E_s/N_0}+\dfrac{6}{(E_s/N_0)^2}+\dfrac{3}{2(E_s/N_0)^3}}\right] \tag{48}$$

or, in terms of bit SNR,

$$S_L = \frac{1}{4}\left[\frac{1}{1+\dfrac{9}{4E_b/N_0}+\dfrac{3}{2(E_b/N_0)^2}+\dfrac{3}{16(E_b/N_0)^3}}\right] \tag{49}$$

Comparing Eq. (49) with Eq. (28), we observe that the suboptimum OQPSK loop based on the MAP implementation for QPSK has a squaring loss that is 6-dB worse than the MAP carrier synchronization loop for QPSK, which itself is significantly inferior at low SNRs to the MAP (optimum) carrier synchronization loop for OQPSK illustrated in Fig. 1. While the suboptimum OQPSK loop has the advantage that its implementation relative to that for QPSK requires only the addition of a $T_s/2$ delay in the quadrature arm, its largely inferior performance coupled with the additional complication of resolving a 90-deg phase ambiguity will no doubt far outweigh the implementation advantage.

VI. Impact on Average Error Probability Performance

The conditional (on a given phase error ϕ) bit-error probability (BEP) of OQPSK is given as the arithmetic average of the conditional bit-error probabilities for BPSK and QPSK, namely (see Appendix E),

$$P_b(E;\phi)|_{OQPSK} = \frac{1}{2}P_b(E;\phi)|_{BPSK} + \frac{1}{2}P_b(E;\phi)|_{QPSK} \tag{50}$$

where [10]

$$\left.\begin{aligned} P_b(E;\phi)|_{BPSK} &= \frac{1}{2}\,\mathrm{erfc}\left(\sqrt{\frac{E_b}{N_0}}\cos\phi\right) \\ P_b(E;\phi)|_{QPSK} &= \frac{1}{4}\,\mathrm{erfc}\left(\sqrt{\frac{E_b}{N_0}}(\cos\phi+\sin\phi)\right)+\frac{1}{4}\,\mathrm{erfc}\left(\sqrt{\frac{E_b}{N_0}}(\cos\phi-\sin\phi)\right) \end{aligned}\right\} \tag{51}$$

As such, for a given phase error (greater than zero), the BEP of OQPSK would be worse than that of BPSK but better than that of QPSK.

When a carrier synchronization loop is used to provide the carrier demodulation reference at the receiver, as considered in this article, then the average bit-error probability (assuming perfect phase ambiguity resolution) would be obtained by averaging Eq. (50) over the probability density function (PDF) of the phase-error process, $p_\phi(\phi)$. For the purpose of comparison, $p_\phi(\phi)$ typically is modeled by a Tikhonov distribution [10,11] with an effective loop SNR, ρ_{eq}, equal to the reciprocal of the variance of

the phase process (2ϕ or 4ϕ as appropriate), the latter being determined from Eq. (18) or Eq. (47). For each of the three modulations, the appropriate relations would be

$$\left.\begin{aligned} p_\phi(\phi)|_{PSK} &= \frac{2\exp(\rho_{eq}\cos 2\phi)}{2\pi I_0(\rho_{eq})}, \quad \rho_{eq} = \frac{\rho S_L|_{PSK}}{4}, \qquad -\frac{\pi}{2} \le \phi \le \frac{\pi}{2} \\ p_\phi(\phi)|_{QPSK} &= \frac{4\exp(\rho_{eq}\cos 4\phi)}{2\pi I_0(\rho_{eq})}, \quad \rho_{eq} = \frac{\rho S_L|_{QPSK}}{16}, \qquad -\frac{\pi}{4} \le \phi \le \frac{\pi}{4} \\ p_\phi(\phi)|_{OQPSK} &= \frac{2\exp(\rho_{eq}\cos 2\phi)}{2\pi I_0(\rho_{eq})}, \quad \rho_{eq} = \frac{\rho S_L|_{OQPSK}}{4}, \quad -\frac{\pi}{2} \le \phi \le \frac{\pi}{2} \end{aligned}\right\} \tag{52}$$

and, thus, the average error probabilities are given by

$$\left.\begin{aligned} P_b(E)|_{BPSK} &= \int_{-\pi/2}^{\pi/2} P_b(E;\phi)|_{BPSK}\, p_\phi(\phi)|_{BPSK}\, d\phi \\ P_b(E)|_{QPSK} &= \int_{-\pi/4}^{\pi/4} P_b(E;\phi)|_{QPSK}\, p_\phi(\phi)|_{QPSK}\, d\phi \\ P_b(E)|_{OQPSK} &= \int_{-\pi/2}^{\pi/2} P_b(E;\phi)|_{OQPSK}\, p_\phi(\phi)|_{OQPSK}\, d\phi \end{aligned}\right\} \tag{53}$$

Note that in the presence of a perfect carrier reference, i.e., $p_\phi(\phi) = \delta(\phi)$, all three modulations would have the identical average bit-error probability.

On the basis of the above relations, we observe that OQPSK offers a two-fold average BEP advantage over QPSK, namely, the conditional BEP is itself smaller and the variance of the phase error that characterizes the PDF of the phase process is considerably smaller for the former relative to the latter. In addition, as previously mentioned, OQPSK needs only to resolve a 180-deg phase ambiguity (e.g., with binary differential encoding/decoding), whereas QPSK needs to resolve a 90-deg phase ambiguity (e.g., with four-phase differential encoding/decoding). This phase ambiguity advantage is particularly significant in error-correction coded communications (e.g., convolutionally coded communications) in that if the code is transparent[10] (reversal of the input bits produces a reversal of the encoder output symbols), one can resolve the phase ambiguity by including a binary differential encoder *before* the convolutional encoder and a binary differential decoder *after* the convolutional decoder. As such, the overall BEP of the coded system is approximately increased by merely a factor of two. When a 90-deg phase ambiguity is present, this simple solution based on the 180-deg transparency of the code is not possible. Instead, either a redesign of the code to achieve, if possible, 90-, 180-, and 270-deg rotational invariance, which, in general, will yield a somewhat poorer performing code, or some other method for resolving the phase ambiguity at the receiver based on the rate of buildup of the convolutional decoder metrics would be required.

[10] In most cases, transparent convolutional codes can be found that have a performance either equal to or nearly equal to that of the optimum code.

VII. Conclusion

OQPSK modulation, which limits the phase variation per transition to 90 deg rather than 180 deg as in QPSK, most often is used on a nonlinear channel to prevent regeneration of the spectral side lobes that have been reduced by bandpass filtering at the transmitter. On a linear channel, OQPSK is employed less often since, in an ideal environment, it is well-known to offer no advantage to QPSK. When the channel is linear but nonideal, i.e., in the presence of a practical carrier synchronizer, we have shown that OQPSK offers both average bit-error probability and phase ambiguity advantages over QPSK with little additional implementation complexity. Although not specifically addressed, the conclusions drawn here also apply to pulse-shaped QPSK and OQPSK since, with matched filters used in the receivers, the performance is invariant to the specific pulse shape. As an example, precoded minimum shift keying (MSK) [10, Chapter 10], which has an equivalent representation in the form of OQPSK with a half-sinusoidal pulse shape, can be carrier synchronized as described in this article.

References

[1] H. Tsou, S. M. Hinedi, and M. K. Simon, "Closed-Loop Carrier Phase Synchronization Techniques Motivated by Likelihood Functions," *The Telecommunications and Data Acquisition Progress Report 42-119, July–September 1994*, Jet Propulsion Laboratory, Pasadena, California, pp. 83–104, November 15, 1994. http://tmo.jpl.nasa.gov/tmo/progress_report/42-119/119S.pdf

[2] W. C. Lindsey and M. K. Simon, "Optimum Performance of Suppressed Carrier Receivers With Costas Loop Tracking," *IEEE Trans. on Comm.*, vol. COM-25, no. 2, pp. 215–227, February 1977.

[3] W. C. Lindsey and M. K. Simon, *Telecommunication Systems Engineering*, Englewood Cliffs, New Jersey: Prentice-Hall, Inc., 1973. Reprinted by Dover Press, New York, 1991.

[4] M. K. Simon, "Optimum Receiver Structures for Phase-Multiplexed Modulations," *IEEE Trans. on Comm.*, vol. COM-26, no. 6, pp. 865–872, June 1978.

[5] M. K. Simon and J. G. Smith, "Carrier Synchronization and Detection of QASK Signal Sets," *IEEE Trans. on Comm.*, vol. COM-22, no. 10, pp. 1576–1584, October 1974.

[6] U. Mengali and A. N. D'Andrea, *Synchronization Techniques for Digital Receivers*, New York: Plenum Press, 1997.

[7] S. Hinedi, "A Functional Description of the Advanced Receiver," *The Telecommunications and Data Acquisition Progress Report 42-100, October–December 1989*, Jet Propulsion Laboratory, Pasadena, California, pp. 131–149, February 15, 1990.

[8] J. B. Berner and K. M. Ware, "An Extremely Sensitive Digital Receiver For Deep Space Communications," Eleventh Annual International Phoenix Conference on Computers and Communications, Phoenix, Arizona, April 1–3, 1992.

[9] J. H. Yuen, ed., *Deep Space Telecommunications Systems Engineering*, New York: Plenum Press, 1983.

[10] M. K. Simon, S. Hinedi, and W. C. Lindsey, *Digital Communication Techniques: Signal Design and Detection*, Englewood Cliffs, New Jersey: Prentice-Hall, Inc., 1994.

[11] V. I. Tikhonov, "The Effect of Noise on Phase-Locked Oscillator Operation," *Automation and Remote Control*, vol. 20, pp. 1160–1168, September 1959. Translated from *Automatika i Telemekhaniki*, Akademya Nauk SSSR, vol. 20, September 1959.

Appendix A

Evaluation of the Correlation Function of the Equivalent Noise Process for the Low SNR Implementation of the MAP Carrier Synchronization Loop for OQPSK

To allow evaluation of the power spectral density of the equivalent additive noise $N_e(t,0)$, we compute here the autocorrelation function $R_{N_e}(\tau) = E\{N_e(t,0)\,N_e(t+\tau,0)\}$ for values of τ corresponding to integer multiples of the baud (symbol) interval T_s. When $\tau = 0$, the variance of $N_e(t,0)$, namely, $R_{N_e}(0) \triangleq R(0) = E\left\{(N_e(t,0))^2\right\}$ is given by Eq. (22) and is evaluated as follows:

$$
\begin{aligned}
R(0) = \\
&4\left[E\left\{(N_1'(1))^2\right\}E\left\{(N_2'(1))^2\right\} + E\left\{(N_1(1))^2\right\}E\left\{(N_2(1))^2\right\} - 2E\{N_1'(1)\,N_1(1)\}\,E\{N_2'(1)\,N_2(1)\}\right] \\
&+ 2PT_s^2\left[E\left\{(N_2'(1))^2\right\} + E\left\{(N_1(1))^2\right\} + E\left\{\left(\frac{a_0+a_1}{2}\right)^2\right\}E\left\{(N_1'(1))^2\right\}\right. \\
&+ E\left\{\left(\frac{b_0+b_{-1}}{2}\right)^2\right\}E\left\{(N_2(1))^2\right\} - 2E\left\{b_0\left(\frac{b_0+b_{-1}}{2}\right)\right\}E\{N_2'(1)\,N_2(1)\} \\
&\left.- 2E\left\{a_0\left(\frac{a_0+a_1}{2}\right)\right\}E\{N_1'(1)\,N_1(1)\}\right] \qquad \text{(A-1)}
\end{aligned}
$$

Recalling the correlation properties of the primed and unprimed noise components,

$$\left.\begin{aligned} N_1(m) &\triangleq \int_{(m-3/2)T_s}^{(m-1/2)T_s} N_s(t)dt \\ N_2(m) &\triangleq \int_{(m-3/2)T_s}^{(m-1/2)T_s} N_c(t)dt \\ N_1'(m) &\triangleq \int_{(m-1)T_s}^{mT_s} N_s(t)dt \\ N_2'(m) &\triangleq \int_{(m-1)T_s}^{mT_s} N_c(t)dt \end{aligned}\right\} \tag{A-2}$$

namely,

$$\left.\begin{aligned} E\left\{\left(N_i'(m)\right)^2\right\} = E\left\{\left(N_i(m)\right)^2\right\} &= \frac{N_0T_s}{2}, \quad i=1,2 \\ E\left\{N_i'(m)N_i(m)\right\} &= \frac{N_0T_s}{4}, \quad i=1,2 \end{aligned}\right\} \tag{A-3}$$

where m is any integer; then substituting Eq. (A-3) into Eq. (A-1) and averaging over the i.i.d. data symbols results in

$$\begin{aligned} R(0) &= 4\left(\frac{3}{8}N_0^2T_s^2\right) + 2PT_s^2\left(N_0T_s\right) \\ &= \frac{3}{2}N_0^2T_s^2\left(1+\frac{4}{3}\frac{PT_s}{N_0}\right) \end{aligned} \tag{A-4}$$

which is given as Eq. (23) of the main text.

When $\tau = T_s$, the cross-correlation $R_{N_e}(T_s) \triangleq R(1) = E\left\{N_e(t,0)\,N_e(t+T_s,0)\right\}$ is given by Eq. (24) and is evaluated as follows:

$$\begin{aligned} R(1) &= 4\left[-E\left\{N_1'(1)\,N_1(2)\right\}E\left\{N_2'(1)\,N_2(2)\right\}\right] \\ &\quad + 2PT_s^2\left[-E\left\{b_0\left(\frac{b_1+b_0}{2}\right)\right\}E\left\{N_2'(1)\,N_2(2)\right\} - E\left\{a_1\left(\frac{a_0+a_1}{2}\right)\right\}E\left\{N_1'(1)\,N_1(2)\right\}\right] \end{aligned} \tag{A-5}$$

Making use of the cross-correlation property of the noise components in different baud intervals given by

$$E\left\{N_i'(m)\,N_i(m+1)\right\} = \frac{N_0T_s}{4}, \quad i=1,2 \tag{A-6}$$

then the equivalent noise correlation in Eq. (A-4) evaluates to

$$R(1) = 4\left(-\frac{1}{16}N_0^2T_s^2\right) + 2PT_s^2\left(-\frac{1}{4}N_0T_s\right)$$

$$= -\frac{1}{4}N_0^2T_s^2\left(1+2\frac{PT_s}{N_0}\right) \tag{A-7}$$

which is given as Eq. (25) of the main text.

Appendix B

Evaluation of the S-Curve of the High SNR Implementation of the MAP Carrier Synchronization Loop for OQPSK

The error signal of the high SNR implementation of the MAP carrier synchronization loop for OQPSK is obtained by substituting Eqs. (10a) and (10b) in Eq. (29), resulting in

$$\begin{aligned} z_1(t) = & \left\{\left[\sqrt{\frac{P}{2}}T_sb_0 - N_1'\right]\sin\phi + \left[\sqrt{\frac{P}{2}}T_s\frac{a_0+a_1}{2} + N_2'\right]\cos\phi\right\} \\ & \times \text{ sgn}\left\{\left[\sqrt{\frac{P}{2}}T_sb_0 - N_1'\right]\cos\phi - \left[\sqrt{\frac{P}{2}}T_s\frac{a_0+a_1}{2} + N_2'\right]\sin\phi\right\} \\ & - \left\{\left[\sqrt{\frac{P}{2}}T_s\frac{b_0+b_{-1}}{2} - N_1\right]\cos\phi - \left[\sqrt{\frac{P}{2}}T_sa_0 + N_2\right]\sin\phi\right\} \\ & \times \text{ sgn}\left\{\left[\sqrt{\frac{P}{2}}T_s\frac{b_0+b_{-1}}{2} - N_1\right]\sin\phi + \left[\sqrt{\frac{P}{2}}T_sa_0 + N_2\right]\cos\phi\right\}, \\ & T_s \le t \le 2T_s \end{aligned} \tag{B-1}$$

which is of the form

$$\begin{aligned} z_1(t) = & \left[X\sin\phi + Y\cos\phi\right] \text{ sgn } \left[X\cos\phi - Y\sin\phi\right] - \left[X'\cos\phi - Y'\sin\phi\right] \text{ sgn } \left\{X'\sin\phi + Y'\cos\phi\right\} \\ \triangleq & \ F_1\left(\phi; X, Y\right) - F_2\left(\phi; X', Y'\right) \end{aligned} \tag{B-2}$$

with X, Y, X', and Y' functions of the data symbols and the noise components. We begin by evaluating the statistical average over the data and noise of $F_1(\phi; X, Y)$. Similar evaluations then will yield the same average of $F_2(\phi; X', Y')$.

Since for a Gaussian zero-mean random variable z with variance σ_z^2,

$$E_z\{\operatorname{sgn}(C+z)\} = \operatorname{erf}\left(\frac{C}{\sqrt{2\sigma_z^2}}\right) \tag{B-3}$$

with C an arbitrary constant, then performing the first average over the noise, we obtain

$$\begin{aligned}\overline{F_1(\phi; X, Y)}^N = \sqrt{\frac{P}{2}}T_s\left(b_0\sin\phi + \frac{a_0+a_1}{2}\cos\phi\right)\operatorname{erf}\left(\sqrt{\frac{E_s}{2N_0}}\left[b_0\cos\phi - \frac{a_0+a_1}{2}\sin\phi\right]\right)\\ - \sin\phi\, E_{N_1'}\left\{N_1'\operatorname{erf}\left(\sqrt{\frac{E_s}{2N_0\sin^2\phi}}\left[b_0\cos\phi - \frac{a_0+a_1}{2}\sin\phi - N_1'\cos\phi\right]\right)\right\}\\ + \cos\phi\, E_{N_2'}\left\{N_2'\operatorname{erf}\left(\sqrt{\frac{E_s}{2N_0\cos^2\phi}}\left[b_0\cos\phi - \frac{a_0+a_1}{2}\sin\phi - N_2'\sin\phi\right]\right)\right\}\end{aligned} \tag{B-4}$$

The remaining averages of the noise can be performed using the relation

$$E_z\{z\operatorname{erf}(A+Bz)\} = \frac{2}{\sqrt{\pi}}\frac{\sigma_z^2 B}{\sqrt{1+2B^2\sigma_z^2}}\exp\left(-\frac{A^2}{1+2B^2\sigma_z^2}\right) \tag{B-5}$$

where again A and B are arbitrary constants. Identifying the Gaussian random variable z as either N_1' or N_2', and then averaging over the data symbols, the first term in Eq. (B-4) finally evaluates to

$$\begin{aligned}E_{a_0,a_1,b_0}\left\{\sqrt{\frac{P}{2}}T_s\left(b_0\sin\phi + \frac{a_0+a_1}{2}\cos\phi\right)\operatorname{erf}\left(\sqrt{\frac{E_s}{2N_0}}\left[b_0\cos\phi - \frac{a_0+a_1}{2}\sin\phi\right]\right)\right\} =\\ \frac{1}{4}\sqrt{\frac{P}{2}}T_s(\sin\phi - \cos\phi)\operatorname{erf}\left(\sqrt{\frac{E_s}{2N_0}}(\cos\phi + \sin\phi)\right)\\ + \frac{1}{4}\sqrt{\frac{P}{2}}T_s(\sin\phi + \cos\phi)\operatorname{erf}\left(\sqrt{\frac{E_s}{2N_0}}(\cos\phi - \sin\phi)\right)\\ + \frac{1}{2}\sqrt{\frac{P}{2}}T_s\sin\phi\operatorname{erf}\left(\sqrt{\frac{E_s}{2N_0}}\cos\phi\right)\end{aligned} \tag{B-6}$$

whereas the second and third terms cancel. Thus, $\overline{F_1(\phi; X, Y)}$ is equal to the expression in Eq. (B-6).

Following a similar approach, it is straightforward to show that the first term in $\overline{F_2(\phi; X, Y)}$ is the negative of the first term in $\overline{F_1(\phi; X, Y)}$, whereas the second and third terms of $\overline{F_2(\phi; X, Y)}$ again cancel. Hence, $\overline{F_2(\phi; X, Y)}$ is evaluated as the negative of the expression in Eq. (B-6). Finally then, from Eq. (B-1), $z_1(t) = 2\overline{F_1(\phi; X, Y)}$, which is twice the result in Eq. (B-6) and thereby agrees with Eq. (30) of the main text.

Appendix C

Evaluation of the Correlation Function of the Equivalent Noise Process for the High SNR Implementation of the MAP Carrier Synchronization Loop for OQPSK

As in Appendix A, to allow evaluation of the power spectral density of the equivalent additive noise $N_e(t,0)$, we compute here the autocorrelation function $R_{N_e}(\tau) = E\{N_e(t,0)\, N_e(t+\tau,0)\}$ for values of τ corresponding to integer multiples of the baud (symbol) interval T_s. When $\tau = 0$, the variance of $N_e(t,0)$, namely, $R_{N_e}(0) \triangleq R(0) = E\left\{(N_e(t,0))^2\right\}$ is obtained from Eq. (33a) as follows:

$$R(0) = 4E\left\{\left(\sqrt{\frac{P}{2}}T_s\frac{a_0+a_1}{2} + N_2'(1)\right)^2\right\} + 4E\left\{\left(\sqrt{\frac{P}{2}}T_s\frac{b_0+b_{-1}}{2} - N_1(1)\right)^2\right\}$$

$$- 8E\left\{\left(\sqrt{\frac{P}{2}}T_s\frac{a_0+a_1}{2} + N_2'(1)\right)\left(\sqrt{\frac{P}{2}}T_s\frac{b_0+b_{-1}}{2} - N_1(1)\right)\right.$$

$$\left.\times \operatorname{sgn}\left[\sqrt{\frac{P}{2}}T_s b_0 - N_1'(1)\right] \operatorname{sgn}\left[\sqrt{\frac{P}{2}}T_s a_0 + N_2(1)\right]\right\} \tag{C-1}$$

Expanding the squared terms and averaging over the data symbols and some of the noise components gives

$$R(0) = 2PT_s^2 + 4N_0T_s - PT_s^2 \operatorname{erf}^2\left(\sqrt{\frac{E_s}{2N_0}}\right)$$

$$+ 4\sqrt{\frac{P}{2}}T_s \operatorname{erf}\left(\sqrt{\frac{E_s}{2N_0}}\right) E\left\{N_1(1)\ \operatorname{sgn}\left[\sqrt{\frac{P}{2}}T_s b_0 - N_1'(1)\right]\right\}$$

$$- 4\sqrt{\frac{P}{2}}T \operatorname{erf}\left(\sqrt{\frac{E_s}{2N_0}}\right) E\left\{N_2'(1)\ \operatorname{sgn}\left[\sqrt{\frac{P}{2}}T_s a_0 + N_2(1)\right]\right\}$$

$$+ 8E\left\{N_1(1)\ \operatorname{sgn}\left[\sqrt{\frac{P}{2}}T_s b_0 - N_1'(1)\right]\right\} E\left\{N_2'(1)\ \operatorname{sgn}\left[\sqrt{\frac{P}{2}}T_s a_0 + N_2(1)\right]\right\} \quad \text{(C-2)}$$

To evaluate the noise expectations in Eq. (C-2), we partition the noise components into two parts, each covering half the integration interval as appropriate. Specifically, let

$$N_1(1) \triangleq \int_{-T_s/2}^{T_s/2} N_s(t)dt = N_{1A}(1) + N_{1B}(1), \quad N_{1A}(1) \triangleq \int_{-T_s/2}^{0} N_s(t)dt, \quad N_{1B}(1) \triangleq \int_0^{T_s/2} N_s(t)dt$$

$$N_2(1) \triangleq \int_{-T_s/2}^{T_s/2} N_c(t)dt = N_{2A}(1) + N_{2B}(1), \quad N_{2A}(1) \triangleq \int_{-T_s/2}^{0} N_c(t)dt, \quad N_{2B}(1) \triangleq \int_0^{T_s/2} N_c(t)dt$$

$$N_1'(1) \triangleq \int_0^{T_s} N_s(t)dt = N_{1B}(1) + N_{1C}(1), \qquad N_{1C}(1) \triangleq \int_{T_s/2}^{T_s} N_s(t)dt$$

$$N_2'(1) \triangleq \int_0^{T_s} N_c(t)dt = N_{2B}(1) + N_{2C}(1), \qquad N_{2C}(1) \triangleq \int_{T_s/2}^{T_s} N_c(t)dt \quad \text{(C-3)}$$

where all the new noise components are independent Gaussian and have variance $N_0T_s/4$. Then, for example, the expectation in the second term of Eq. (C-2) can be written as

$$E\left\{(N_{1A}(1) + N_{1B}(1))\ \operatorname{sgn}\left[\sqrt{\frac{P}{2}}T_s b_0 - (N_{1B}(1) + N_{1C}(1))\right]\right\}$$

$$= E\left\{N_{1B}(1) \operatorname{sgn}\left[\sqrt{\frac{P}{2}}T_s b_0 - (N_{1B}(1) + N_{1C}(1))\right]\right\}$$

$$= E\left\{N_{1B}(1) \operatorname{erf}\left[\frac{\sqrt{\frac{P}{2}}T_s b_0 - N_{1B}(1)}{\sqrt{N_0T_s/2}}\right]\right\} \quad \text{(C-4)}$$

which, using Eq. (B-5) of Appendix B, evaluates to

$$E\left\{N_1(1)\ \operatorname{sgn}\left[\sqrt{\frac{P}{2}}T_s b_0 - N_1'(1)\right]\right\} = -\sqrt{\frac{N_0T_s}{4\pi}} \exp\left(-\frac{E_s}{2N_0}\right) \quad \text{(C-5)}$$

Similarly, the expectation in the third term of Eq. (C-2) evaluates to

$$E\left\{N_2'(1)\ \mathrm{sgn}\left[\sqrt{\frac{P}{2}}T_s a_0 + N_2(1)\right]\right\} = \sqrt{\frac{N_0 T_s}{4\pi}}\exp\left(-\frac{E_s}{2N_0}\right) \tag{C-6}$$

Finally, using Eqs. (C-5) and (C-6) in Eq. (C-2), we get the desired result, namely,

$$\begin{aligned} R(0) &= 2PT_s^2 + 4N_0T_s - PT_s^2\,\mathrm{erf}^2\left(\sqrt{\frac{E_s}{2N_0}}\right) \\ &\quad - 8\sqrt{\frac{P}{2}}T_s\mathrm{erf}\left(\sqrt{\frac{E_s}{2N_0}}\right)\sqrt{\frac{N_0T_s}{4\pi}}\exp\left(-\frac{E_s}{2N_0}\right) - 8\left(\frac{N_0T_s}{4\pi}\right)\exp^2\left(-\frac{E_s}{2N_0}\right) \end{aligned} \tag{C-7}$$

which, upon simplification, results in the first equation in Eq. (34).

Analogous to Eq. (C-1) for $\tau = T_s$, the correlation $R_{N_e}(T_s) \triangleq R(1) = E\{N_e(t,0)\,N_e(t+T_s,0)\}$ is obtained from Eq. (33b) as

$$\begin{aligned} R(1) &= 4E\left\{\left(\sqrt{\frac{P}{2}}T_s\frac{a_0+a_1}{2} + N_2'(1)\right)\right. \\ &\quad \left.\times\left(\sqrt{\frac{P}{2}}T_s\frac{a_1+a_2}{2} + N_2'(2)\right)\mathrm{sgn}\left[\sqrt{\frac{P}{2}}T_sb_0 - N_1'(1)\right]\mathrm{sgn}\left[\sqrt{\frac{P}{2}}T_sb_1 - N_1'(2)\right]\right\} \\ &\quad - 4E\left\{\left(\sqrt{\frac{P}{2}}T_s\frac{a_0+a_1}{2} + N_2'(1)\right)\right. \\ &\quad \left.\times\left(\sqrt{\frac{P}{2}}T_s\frac{b_1+b_0}{2} - N_1(2)\right)\mathrm{sgn}\left[\sqrt{\frac{P}{2}}T_sb_0 - N_1'(1)\right]\mathrm{sgn}\left[\sqrt{\frac{P}{2}}T_sa_1 + N_2(2)\right]\right\} \\ &\quad - 4E\left\{\left(\sqrt{\frac{P}{2}}T_s\frac{b_0+b_{-1}}{2} - N_1(1)\right)\right. \\ &\quad \left.\times\left(\sqrt{\frac{P}{2}}T_s\frac{a_1+a_2}{2} + N_2'(2)\right)\mathrm{sgn}\left[\sqrt{\frac{P}{2}}T_sa_0 + N_2(1)\right]\mathrm{sgn}\left[\sqrt{\frac{P}{2}}T_sb_1 - N_1'(2)\right]\right\} \\ &\quad + 4E\left\{\left(\sqrt{\frac{P}{2}}T_s\frac{b_0+b_{-1}}{2} - N_1(1)\right)\right. \\ &\quad \left.\times\left(\sqrt{\frac{P}{2}}T_s\frac{b_1+b_0}{2} - N_1(2)\right)\mathrm{sgn}\left[\sqrt{\frac{P}{2}}T_sa_0 + N_2(1)\right]\mathrm{sgn}\left[\sqrt{\frac{P}{2}}T_sa_1 + N_2(2)\right]\right\} \end{aligned} \tag{C-8}$$

When performing the required averages over the data symbols and noise components, the first term in Eq. (C-8) evaluates as

$$4E\left\{\left(\sqrt{\frac{P}{2}}T_s\frac{a_0+a_1}{2}+N_2'(1)\right)\right.$$

$$\left.\times\left(\sqrt{\frac{P}{2}}T_s\frac{a_1+a_2}{2}+N_2'(2)\right)\text{sgn}\left[\sqrt{\frac{P}{2}}T_sb_0-N_1'(1)\right]\text{sgn}\left[\sqrt{\frac{P}{2}}T_sb_1-N_1'(2)\right]\right\}$$

$$=2PT_s^2E\left\{b_0\left(\frac{a_0+a_1}{2}\right)b_1\left(\frac{a_1+a_2}{2}\right)\right\}\text{erf}^2\left(\sqrt{\frac{E_s}{2N_0}}\right)=0 \tag{C-9}$$

To evaluate the second term in Eq. (C-8), we again must partition each of the noise components into two parts, as in Eq. (C-3), and then perform the necessary averages. When this is done, we obtain

$$-4E\left\{\left(\sqrt{\frac{P}{2}}T_s\frac{a_0+a_1}{2}+N_2'(1)\right)\right.$$

$$\left.\times\left(\sqrt{\frac{P}{2}}T_s\frac{b_1+b_0}{2}-N_1(2)\right)\text{sgn}\left[\sqrt{\frac{P}{2}}T_sb_0-N_1'(1)\right]\text{sgn}\left[\sqrt{\frac{P}{2}}T_sa_1+N_2(2)\right]\right\}$$

$$=-2N_0T_s\left[\sqrt{\frac{E_s}{4N_0}}\text{erf}\left(\sqrt{\frac{E_s}{2N_0}}\right)+\sqrt{\frac{1}{2\pi}}\exp\left(-\frac{E_s}{2N_0}\right)\right]^2 \tag{C-10}$$

Because of the independence of the noise components in each factor of the third and fourth terms in Eq. (C-8), each expectation partitions into a four-fold product of expectations, e.g.,

$$-4E\left\{\left(\sqrt{\frac{P}{2}}T_s\frac{b_0+b_{-1}}{2}-N_1(1)\right)\right.$$

$$\left.\times\left(\sqrt{\frac{P}{2}}T_s\frac{a_1+a_2}{2}+N_2'(2)\right)\text{sgn}\left[\sqrt{\frac{P}{2}}T_sa_0+N_2(1)\right]\text{sgn}\left[\sqrt{\frac{P}{2}}T_sb_1-N_1'(2)\right]\right\}$$

$$=-4E\left\{\left(\sqrt{\frac{P}{2}}T_s\frac{b_0+b_{-1}}{2}-N_1(1)\right)\right\}E\left\{\sqrt{\frac{P}{2}}T_s\frac{a_1+a_2}{2}+N_2'(2)\right\}$$

$$\times E\left\{\text{sgn}\left[\sqrt{\frac{P}{2}}T_sa_0+N_2(1)\right]\right\}E\left\{\text{sgn}\left[\sqrt{\frac{P}{2}}T_sb_1-N_1'(2)\right]\right\}=0 \tag{C-11}$$

Similarly,

$$4E\left\{\left(\sqrt{\frac{P}{2}}T_s\frac{b_0+b_{-1}}{2}-N_1\left(1\right)\right)\right.$$

$$\left.\times\left(\sqrt{\frac{P}{2}}T_s\frac{b_1+b_0}{2}-N_1\left(2\right)\right)\,\mathrm{sgn}\left[\sqrt{\frac{P}{2}}T_sa_0+N_2\left(1\right)\right]\,\mathrm{sgn}\left[\sqrt{\frac{P}{2}}T_sa_1+N_2\left(2\right)\right]\right\}$$

$$=4E\left\{\left(\sqrt{\frac{P}{2}}T_s\frac{b_0+b_{-1}}{2}-N_1\left(1\right)\right)\right\}E\left\{\sqrt{\frac{P}{2}}T_s\frac{b_1+b_0}{2}-N_1\left(2\right)\right\}$$

$$\times E\left\{\mathrm{sgn}\left[\sqrt{\frac{P}{2}}T_sa_0+N_2\left(1\right)\right]\right\}E\left\{\mathrm{sgn}\left[\sqrt{\frac{P}{2}}T_sa_1+N_2\left(2\right)\right]\right\}=0 \tag{C-12}$$

Finally, combining Eqs. (C-9) through (C-12), we obtain the desired result for the cross-correlation $R(1)$, namely,

$$R(1)=-2N_0T_s\left[\sqrt{\frac{E_s}{4N_0}}\mathrm{erf}\left(\sqrt{\frac{E_s}{2N_0}}\right)+\sqrt{\frac{1}{2\pi}}\exp\left(-\frac{E_s}{2N_0}\right)\right]^2 \tag{C-13}$$

which agrees with the second equation of Eq. (34).

Appendix D

Evaluation of the Correlation Function of the Equivalent Noise Process for the Low SNR Implementation of the Suboptimum Carrier Synchronization Loop for OQPSK

Expanding the terms in Eq. (44) of the main text and combining like terms, we arrive at the following expressions for the equivalent additive noise, $N_e(t,0)$, where we again have introduced the parenthetical notation to distinguish the noise components in two successive baud intervals:

$$N_e(t,0) = 4\left[-2\left(\frac{P}{2}\right)^{3/2} T_s^3\left[b_{-1}N_2(1) + a_0 N_1'(1)\right] - 3\frac{P}{2}a_0 b_{-1}T_s^2\left[(N_2(1))^2 - (N_1'(1))^2\right]\right.$$

$$+\left(\frac{P}{2}\right)^{1/2} T_s\left[3b_{-1}N_2(1)(N_1'(1))^2 + 3a_0 N_1'(1)(N_2(1))^2 - a_0(N_1'(1))^3 - b_{-1}(N_2(1))^3\right]$$

$$\left.+N_1'(1)(N_2(1))^3 - N_2(1)(N_1'(1))^3\right],$$

$$\frac{T_s}{2} \le t \le \frac{3T_s}{2} \qquad \text{(D-1a)}$$

$$N_e(t,0) = 4\left[-2\left(\frac{P}{2}\right)^{3/2} T_s^3\left[b_0 N_2(2) + a_1 N_1'(2)\right] - 3\frac{P}{2}T_s^2 a_1 b_0\left[(N_2(2))^2 - (N_1'(2))^2\right]\right.$$

$$+\left(\frac{P}{2}\right)^{1/2} T_s\left[3b_0 N_2(2)(N_1'(2))^2 + 3a_1 N_1'(2)(N_2(2))^2 - a_1(N_1'(2))^3 - b_0(N_2(2))^3\right]$$

$$\left.+N_1'(2)(N_2(2))^3 - N_2(2)(N_1'(2))^3\right],$$

$$\frac{3T_s}{2} \le t \le \frac{5T_s}{2} \qquad \text{(D-1b)}$$

The variance of $N_e(t,0)$, namely, $R_{N_e}(0) \triangleq R(0) = E\left\{(N_e(t,0))^2\right\}$ is evaluated after some simplification and combining of terms as

$$R(0) =$$

$$16\left[4\left(\frac{P}{2}\right)^3 T_s^6\left[E\left\{\left(N_2(1)\right)^2\right\}+E\left\{\left(N_1'(1)\right)^2\right\}\right]\right.$$

$$+\left(\frac{P}{2}\right)^2 T_s^4\left[13E\left\{\left(N_2(1)\right)^4\right\}+13E\left\{\left(N_1'(1)\right)^4\right\}-42E\left\{\left(N_2(1)\right)^2\right\}E\left\{\left(N_1'(1)\right)^2\right\}\right]+\frac{P}{2}T_s^2$$

$$\times\left[3E\left\{\left(N_1'(1)\right)^2\right\}E\left\{\left(N_2(1)\right)^4\right\}+3E\left\{\left(N_2(1)\right)^2\right\}E\left\{\left(N_1'(1)\right)^4\right\}+E\left\{\left(N_2(1)\right)^6\right\}+E\left\{\left(N_1'(1)\right)^6\right\}\right]$$

$$\left.+E\left\{\left(N_1'(1)\right)^2\right\}E\left\{\left(N_2(1)\right)^6\right\}+E\left\{\left(N_2(1)\right)^2\right\}E\left\{\left(N_1'(1)\right)^6\right\}-2E\left\{\left(N_2(1)\right)^4\right\}E\left\{\left(N_1'(1)\right)^4\right\}\right] \quad \text{(D-2)}$$

Using the well-known relation for the even-ordered moments of a zero-mean Gaussian random variable, z, namely,

$$E\{z^n\} = (n-1)!!\sigma_z^n \quad \text{(D-3)}$$

where $(n-1)!!$ denotes the factorial made up of only odd integers, then Eq. (D-2) finally evaluates to

$$R(0) = 64\left[\left(\frac{P}{2}\right)^3 N_0 T_s^7+\frac{9}{4}\left(\frac{P}{2}\right)^2 N_0^2 T_s^6+\frac{3}{2}\left(\frac{P}{2}\right)N_0^3 T_s^5+\frac{3}{16}N_0^4 T_s^4\right]$$

$$= 8\left[P^3 N_0 T_s^7+\frac{9}{2}P^2 N_0^2 T_s^6+6PN_0^3 T_s^5+\frac{3}{2}N_0^4 T_s^4\right] \quad \text{(D-4)}$$

Next, multiplying Eqs. (D-1a) and (D-1b) and first averaging over the signal (i.i.d. data symbols) gives

$$E_s\{N_e(t,0)\,N_e(t+T_s,0)\}$$

$$= 16E\left\{\left[N_1'(1)\left(N_2(1)\right)^3-N_2(1)\left(N_1'(1)\right)^3\right]\left[N_1'(2)\left(N_2(2)\right)^3-N_2(2)\left(N_1'(2)\right)^3\right]\right\}$$

$$= 16\left[E\{N_1'(1)\,N_1'(2)\}E\left\{\left(N_2(1)\right)^3\left(N_2(2)\right)^3\right\}+E\{N_2(1)\,N_2(2)\}E\left\{\left(N_1'(1)\right)^3\left(N_1'(2)\right)^3\right\}\right.$$

$$\left.-E\left\{N_2(1)\left(N_2(2)\right)^3\right\}E\left\{\left(N_1'(1)\right)^3 N_1'(2)\right\}-E\left\{\left(N_2(1)\right)^3 N_2(2)\right\}E\left\{N_1'(1)\left(N_1'(2)\right)^3\right\}\right] \quad \text{(D-5)}$$

Finally, because of the independence of the noise components in adjacent baud intervals, each term in Eq. (D-5), when averaged over these components, equals zero. Thus, $R(1) = 0$.

Appendix E

Evaluation of the Conditional Bit-Error Probability for OQPSK

Consider the optimum (matched -filter) receiver for OQPSK, which makes independent hard decisions on the I and Q data symbol streams. The output of the I matched filter corresponding to the transmitted bit a_0 [see Eq. (2)] is given by

$$\begin{aligned} X_I &\triangleq \int_{-T_s/2}^{T_s/2} \left(s\left(t,\theta\right)+n(t)\right) r_I\left(t\right) dt \\ &= \int_{-T_s/2}^{T_s/2} \sqrt{P}\left(a_0\cos\left(\omega_c t+\theta\right)+\left(\frac{b_{-1}+b_0}{2}\right)\sin\left(\omega_c t+\theta\right)\right)\sqrt{2}\cos\left(\omega_c t+\hat{\theta}\right) dt \\ &\quad + \int_{-T_s/2}^{T_s/2} \sqrt{2}\left[N_c(t)\cos\left(\omega_c t+\theta\right)-N_s(t)\sin\left(\omega_c t+\theta\right)\right]\sqrt{2}\cos\left(\omega_c t+\hat{\theta}\right) dt \\ &= \sqrt{\frac{P}{2}}T_s\left(a_0\cos\phi+\left(\frac{b_{-1}+b_0}{2}\right)\sin\phi\right)+N_I\cos\phi-N_Q\sin\phi \end{aligned} \tag{E-1}$$

where

$$\left.\begin{aligned} N_I &\triangleq \int_{-T_s/2}^{T_s/2} N_c(t)dt \\ N_Q &\triangleq \int_{-T_s/2}^{T_s/2} N_s(t)dt \end{aligned}\right\} \tag{E-2}$$

which are independent zero-mean Gaussian random variables each with variance $\sigma_N^2 = N_0T_s/2$. Making a binary hard decision on X_I results in the decision on a_0. Hence, the probability of error associated with a_0 is computed as follows. Assuming a +1 transmitted symbol for a_0, the conditional (on the phase error ϕ) probability of error is

$$\begin{aligned} \Pr\left\{\hat{a}_0=-1\,|a_0=1;\phi\right\} &= \Pr\left\{X_I<0\,|a_0=1\right\} = \overline{\frac{1}{2}\mathrm{erfc}\left\{\frac{X_I\,|a_0=1}{\sqrt{2}\sigma_{X_I}}\right\}}^{b_{-1},b_0} \\ &= \overline{\frac{1}{2}\mathrm{erfc}\left\{\sqrt{\frac{PT_s}{2N_0}}\left[\cos\phi+\left(\frac{b_{-1}+b_0}{2}\right)\sin\phi\right]\right\}}^{b_{-1},b_0} \end{aligned} \tag{E-3}$$

where the overbar denotes statistical averaging over the equiprobable quadrature binary symbols that interfere with the in-phase bit a_0. Since

$$\frac{b_{-1}+b_0}{2} = \begin{cases} 0, & b_{-1} = -b_0 \text{ with probability} = \dfrac{1}{2} \\ -1, & b_{-1} = b_0 = -1 \text{ with probability} = \dfrac{1}{4} \\ 1, & b_{-1} = b_0 = 1 \text{ with probability} = \dfrac{1}{4} \end{cases} \tag{E-4}$$

then further noting that $PT_s/2N_0 = PT_b/N_0 \triangleq E_b/N_0$, the average probability of error in Eq. (E-3) becomes

$$\Pr\{\hat{a}_0 = -1 \,|a_0 = 1; \phi\} = \frac{1}{4}\text{erfc}\left[\sqrt{\frac{PT_s}{2N_0}}\cos\phi\right] + \frac{1}{8}\text{erfc}\left[\sqrt{\frac{PT_s}{2N_0}}(\cos\phi + \sin\phi)\right]$$

$$+ \frac{1}{8}\text{erfc}\left[\sqrt{\frac{PT_s}{2N_0}}(\cos\phi - \sin\phi)\right] \tag{E-5}$$

Because of the symmetry of the problem, the result for $\Pr\{\hat{a}_0 = 1 \,|a_0 = -1; \phi\}$ would be identical to that in Eq. (E-5). Thus, the average probability of error, $P_I(E)$, for detecting the I-channel symbols is given by the right-hand side of Eq. (E-5). Again by the symmetry of the problem, the identical expression to Eq. (E-5) would be obtained for the average probability of error associated with the Q-channel symbols. Finally, the average bit-error probability (still conditioned on ϕ), $P_b(E;\phi)$, corresponding to the sequence obtained by interleaving the I- and Q-channel symbol decisions, also is given by Eq. (E-5), namely,

$$P_b(E;\phi) = \frac{1}{4}\text{erfc}\left[\sqrt{\frac{PT_s}{2N_0}}\cos\phi\right] + \frac{1}{8}\text{erfc}\left[\sqrt{\frac{PT_s}{2N_0}}(\cos\phi + \sin\phi)\right]$$

$$+ \frac{1}{8}\text{erfc}\left[\sqrt{\frac{PT_s}{2N_0}}(\cos\phi - \sin\phi)\right] \tag{E-6}$$

which can be put in the form of Eq. (50) combined with Eq. (51).